Synthesis of Au nanoparticle doped SiO_2–TiO_2 films: tuning of Au surface plasmon band position through controlling the refractive index†

Samar Kumar Medda, Sucheta De and Goutam De*

Received 6th May 2005, Accepted 23rd June 2005
First published as an Advance Article on the web 5th July 2005
DOI: 10.1039/b506399j

The position of the surface plasmon resonance (SPR) band of Au nanoparticles was tailored by controlling the refractive indices (n) of the embedding matrices, to develop different coloured coatings on glass substrates. Five sets of Au nanoparticle doped coatings were prepared from sols derived from tetraethyl orthosilicate–3-(glycidoxypropyl)trimethoxysilane–titanium tetraethoxide containing gold chloride, following a sol-gel dip-coating method. The film samples of nominal formula $(SiO_2)_x(TiO_2)_{0.97-x}Au_{0.03}$ (x = 0.97, 0.679, 0.485, 0.388 and 0.242) were prepared after heat treatment at 500 °C in air. The Au SPR peak, in the case of a SiO_2 host (SiO_2 : TiO_2 = 1 : 0, n = 1.411), observed at 542 nm, gradually red-shifted to 600 nm upon increasing the TiO_2 content (SiO_2 : TiO_2 = 1 : 3, n = 1.939). As a consequence, a systematic change of the Au SPR position yielded pink, magenta, violet, royal and blue coloured coatings on ordinary sheet glasses. The formation of Au nanoparticles in the above gel and glassy coating matrices was monitored by UV–visible and FTIR spectroscopy, X-ray diffraction and transmission electron microscopy.

Introduction

The optical absorption position of metal nanoparticles (*e.g.* Au, Ag, Cu *etc.*) which are much smaller than the wavelength of light can be tailored by controlling several factors like shape, size, composition and concentration of the nanoparticles[1–9], and the refractive index (n) of the embedding medium.[5,10,11] According to Mie theory[12] the optical absorption α of metal nanoparticles embedded in a medium of refractive index n is:[12,13]

$$\alpha = \frac{18\pi Q n^3 \varepsilon_2 / \lambda}{(\varepsilon_1 + 2n^2)^2 + \varepsilon_2^2}$$

where Q is the volume fraction of nanoparticles and ε_1 and ε_2 are the cluster-size dependent dielectric constants which are functions of radius (r) and wavelength (λ). Therefore, if the size, shape and concentration of the nanoparticles are more or less similar in the embedding matrices, the absorption position due to SPR in the visible wavelength region can be tailored by changing the n of the matrices. Based on this, we attempted to synthesize different coloured coatings using dispersed Au nanoparticles of fixed molar concentration in dielectric hosts (SiO_2 and mixed SiO_2–TiO_2) having different values of n. It may also be noted here that metal nanocrystals embedded in appropriate glassy hosts are also known to exhibit enhanced nonlinear optical properties, with a large intensity-dependent refractive index related to the real part of the third-order susceptibility, $\chi^{(3)}$.[14] Such coating materials could also have potential optoelectronic applications in optical switching and limiting devices because of the ultrafast nonlinear response.[14–16] The aim of this work was therefore two fold: (i) synthesis and characterisation of Au nanoparticles in SiO_2 and mixed SiO_2–TiO_2 thin film hosts which could be utilised as nonlinear optical materials and (ii) to study the effect of the matrix refractive index (n) on the optical properties of Au nanoparticles, leading to the generation of different colours useful for indoor and outdoor decorative purposes.

An earlier report[17] shows that it is difficult to incorporate a large concentration of Au in a SiO_2 host and that methyl triethoxysilane used with tetraethyl orthosilicate could incorporate Au nanoparticles with a Au : Si atomic ratio of 0.048. Even at this concentration, it was reported that some Au crystallites had migrated to the surface of the coatings and eventually come out of the matrix as a light brown precipitate after heat treatment.[17] For this reason intense and uniform coloration of the coatings could not be achieved for any practical applications. Furthermore, with a higher concentration of Au there is a greater probability of agglomeration, resulting in wide size distribution of clusters. It is also known that with the conventional alkoxide derived sols relatively thicker coatings cannot be obtained by a single dipping. The coatings suffer from catastrophic cracking and detachment from the substrate after heat treatment if the thickness is greater than 500 nm, in case of SiO_2, or 100 nm, in case of TiO_2. The cracking can be overcome by using organically modified silicon alkoxide precursors. In the present work, therefore, we kept the Au concentration low (Au/oxide = 0.03) to avoid agglomeration and migration of Au nanoparticles and maintained an optimum level of coating thickness after heat treatment using SiO_2 and the TiO_2–ormosil (inorganic–organic hybrid) approach.[18]

Experimental

Preparation of sols

All chemicals were used as received. Tetraethyl orthosilicate (TEOS), 3-(glycidoxypropyl)trimethoxysilane (GLYMO) and

Sol-Gel Division, Central Glass and Ceramic Research Institute, 196, Raja S.C. Mullick Road, Kolkata 700 032, India.
E-mail: gde@cgcri.res.in

† Electronic supplementary information (ESI) available: XRD spectra of Au doped films. See http://dx.doi.org/10.1039/b506399j

Table 1 Mol ratios of different alkoxides used to prepare sols

Sample label	TEOS (mol)	GLYMO (mol)	TTE (mol)
ST10	7	3	0
ST73	4	3	3
ST55	2	3	5
ST46	1	3	6
ST39	0	3	9

titanium tetraethoxide (TTE) were supplied by Sigma-Aldrich, while $HAuCl_4 \cdot 3H_2O$, *n*-butanol, HCl and acetylacetone (acac) were obtained from SD Fine-Chem Ltd. Aluminum acetylacetonate ($Al(acac)_3$) was supplied by Lancaster.

Five sets of Au nanoparticle doped SiO_2 and SiO_2–TiO_2 coatings on ordinary soda-lime glass substrates were prepared. First, undoped hybrid sols were prepared using TEOS, GLYMO, TTE, acac, $Al(acac)_3$ (a catalytic amount as an epoxy polymerization initiator), *n*-butanol, water and a catalytic amount of HCl. The alkoxides TEOS, GLYMO and TTE were used in different mol ratios (Table 1) in order to obtain different SiO_2–TiO_2 contents in the final heat treated coatings. First, a TTE-acac solution was prepared by stirring (30 min) the required amount of TTE with acac (0.5 mol per Ti-alkoxide) in *n*-butanol (one-third of the total amount). TEOS, GLYMO and TTE–acac solution in the required proportions were then mixed with *n*-butanol (one-third of total amount) by stirring and refluxed for 30 min in order to obtain a homogeneous solution. The solution was then cooled to room temperature. Acidulated water dissolved in *n*-butanol (the remaining one-third) was then added while stirring; stirring was continued for 1 h. 5×10^{-4} mol HCl and 0.5 mol water per mol of alkoxy group were used for hydrolysis/condensation reactions. The epoxy polymerizing agent $Al(acac)_3$ (0.05 mol per mol of GLYMO) was added at this stage, stirring until it dissolved.[19] The resulting clear sols, having five different compositions as shown in Tables 1 and 2, were then used for Au doping. The equivalent oxide (SiO_2 + TiO_2) wt.% in the sols was in the range 12–16%. The molar ratio of the Au metal to the oxide (SiO_2 + TiO_2) was kept constant in all the sols at 3 equivalent mol% Au to 97% oxide (SiO_2 + TiO_2). The calculated amount of $HAuCl_4 \cdot 3H_2O$ was dissolved in water (the molar ratio of water to $HAuCl_4 \cdot 3H_2O$ can be varied from 10–12) and added to the corresponding undoped sols while stirring. In the case of TiO_2 containing sols, a faint turbidity appeared after the addition of the $HAuCl_4 \cdot 3H_2O$ solution. This precipitation can be dissolved by adding a few drops of concentrated HCl–*n*-butanol mixture (1 : 1 by volume). The clear yellow sols thus obtained were used for the preparation of coatings.

Table 2 Refractive indices of the heat treated undoped films

Label[a]	SiO_2 : TiO_2 mol ratio	n_{meas} (at 550 nm)	
		90 °C	500 °C
ST10	1 : 0	1.468	1.411
ST73	1 : 0.43	1.545	1.604
ST55	1 : 1	1.593	1.713
ST46	1 : 1.5	1.626	1.862
ST39	1 : 3	1.648	1.939

[a] Same sample label corresponding to the Au-doped films were used. These undoped films of thickness ranges from 30–50 nm were prepared for the measurement of refractive index values.

Preparation of coatings

The Au-doped coatings were deposited on 1 mm thick, clean soda-lime–silica glass substrates. Prior to the coating deposition, the glass substrates were cleaned with a warm neutral detergent solution, rinsed with distilled water and isopropanol and finally, boiled in isopropanol for 5 min. The coatings were prepared using the dipping technique (Dip-master 200, Chemat Corporation) with withdrawal velocities in the range 1–3 in min^{-1}. Similar Au-doped coatings on silicon wafers (both sides polished) were prepared for the IR spectral studies. The as-prepared coatings were first dried at 60 °C for 60 min, then at 90 °C for a further 60 min. The dried films were then heated (heating rate 75 °C h^{-1}) to 500 °C with a soaking time of 30 min. Undoped coatings in the range 30–50 nm thick were also prepared on silicon wafers for the measurement of matrix refractive index values. The thickness of the heat treated Au-doped coatings was measured by a Surfcorder SE-2300 profilometer (Kosaka Laboratory Ltd., Japan). Infrared absorption spectra of the films deposited on silicon wafers were recorded by FTIR spectrometry (Nicolet, model 5PC) with a resolution of 4 cm^{-1} and 200 scans for each sample. The UV–visible spectra of the coatings deposited on soda-lime–silica glass substrates were obtained using a Cary 50 scan spectrophotometer. Powder X-ray diffraction (XRD) patterns of the coatings were recorded with a diffractometer, operating at 40 kV and 30 mA using Ni-filtered Cu K_α radiation. Transmission electron microscope (TEM) measurements were carried out on a JEOL 2010. The refractive indices were measured using a J. A. Wollam Co. M44 spectroscopic ellipsometer. All refractive indices were reported at a wavelength of 550 nm.

Results and discussions

In order to obtain different refractive indices for the coatings, the mole ratio of SiO_2 to TiO_2 was varied using TEOS and GLYMO (the source of SiO_2) and TTE (the source of TiO_2) (Table 1). As expected, after heat treatment of the coatings the refractive indices increased with increasing Ti-component (Table 2). Tailoring the refractive index (*n*) by SiO_2 : TiO_2 composition control shows an approximately linear dependence which roughly obeys the rule of mixtures.[20] Note that the refractive indices obtained in this work are low compared to those of previously reported SiO_2–TiO_2 mixed films of similar molar compositions. This is due to a larger volume fraction of the crystalline TiO_2 phase in the previously reported films. A low refractive index is an indication that our films are porous and amorphous in nature.

All as-prepared Au doped coatings were clear and transparent. All coatings showed very uniform intense coloration after heat treatment at 500 °C in air. The nominal compositions of the Au-doped coatings of general formula $(SiO_2)_x(TiO_2)_{0.97-x}Au_{0.03}$ (x = 0.97, 0.679, 0.485, 0.388 and 0.242) and their colours and corresponding Au SPR positions are presented in Table 3. It has been observed that the use of

Table 3 Nominal compositions of the heat treated (500 °C) films, $(SiO_2)_x(TiO_2)_{0.97-x}Au_{0.03}$ with their colour and SPR peak positions

				Nominal composition of the heat treated coatings (mol%)		
Sample label	Film colour	Au SPR Position/nm	x SiO_2	SiO_2	TiO_2	Au
ST10	Pink	542	0.970	97.0	0	3
ST73	Magenta	555	0.679	67.9	29.1	3
ST55	Violet	572	0.485	48.5	48.5	3
ST46	Royal	580	0.388	38.8	58.2	3
ST39	Blue	600	0.242	24.25	72.75	3

GLYMO with TEOS and TTE helped to increase the thickness of the coatings and prevent cracking after heat treatment at 500 °C. No Au precipitation was observed on the surface of the dried and heated coatings indicating that all Au nanoparticles are trapped inside the coating matrices.[17] We therefore consider that the nominal compositions mentioned above are maintained in these films. The coating thickness of the heat treated (500 °C) films, estimated by a profilometer, was in the 250–600 nm range. The adhesion and hardness of the coatings was also found to be excellent. The pencil hardness value (measured following the specifications of ASTM D 3363) of the heat treated (500 °C) coatings is greater than 9H and no scratch mark was observed on the coatings after rubbing the coating surfaces with #000 grade steel wool. These results confirmed that the coatings adhere strongly to the substrates and are sufficiently hard for any practical uses.

Fig. 1 (a–c) shows the FTIR spectra of dried and heat treated Au-doped ST10 and a representative Ti-containing film, ST55. FTIR of as-prepared ST10 (Fig. 1a) film shows peaks corresponding to Si–O–Si (asymmetric stretch) overlapping with Si–O–C at around 1090 cm^{-1}, Si–OH at 942 cm^{-1},[21,22] epoxide ring vibrations at 910 and 855 cm^{-1} (shoulder),[23] Si–O–Si (symmetric stretch) at 795 cm^{-1} and 448 cm^{-1}.[21,22] In case of dried films (60 °C and 90 °C), all bands were unaffected except the epoxide bands (910 and 855 cm^{-1}) which gradually weakened and almost disappeared at 90 °C due to polymerization of epoxy groups to poly(ethylene oxide).[23] It may be pointed out here that under acidic conditions (the hydrolysis reaction was initiated in an acidic medium and later $HAuCl_4$ was used as gold source), the epoxy group may react with water to form diols which cannot be further polymerised to poly(ethylene oxide). In the FTIR spectra of all dried (60° and 90 °C) films, no diol vibration band at 4080 cm^{-1} was observed. The absence of epoxide and diol vibrations indicates the complete polymerisation of epoxide groups after drying at 90 °C.[21,23] As we used acac to control the fast hydrolysis rate of Ti-alkoxide, FTIR spectra of all as-prepared and dried Ti-containing film samples showed a sharp pair of peaks at 1585 and 1530 cm^{-1} due to CC+CO stretching[24] arising from Ti–acac chelate. The presence of bands in the 1385–1260 cm^{-1} region and at 670 cm^{-1}, all attributed to the Ti–O–C vibrations, also supports that acac is bonded to Ti as chelating ligand.[18] In the FTIR spectra of as-prepared and dried ST55 film (Fig. 1b), the Ti-acac chelate related bands are marked by asterisk. In this case, we also observe epoxide ring vibrations at about 910 and 855 cm^{-1}. The presence of bands at around 930 and 750 cm^{-1} confirms the formation of a Si–O–Ti network. The intensities of acac related peaks are gradually weakened during drying (up to 90 °C) and completely vanished after heat treatment at 500 °C. The epoxide bands also disappeared at 90 °C due to polymerization. FTIR spectra of heat treated (500 °C and 700 °C) ST10 and ST55 films are shown in Fig. 1c to illustrate the formation of the Si–O–Ti network. The heat treated (500 °C) ST10 (pure silica) film shows Si–O–Si vibrations at 1072, 805 and 455 cm^{-1} and a weak peak due to Si–OH at 962 cm^{-1}. The corresponding ST55 film shows Si–O–Si vibrations at 1058, 796 and 455 cm^{-1} and Si–O–Ti at 935 and 750 cm^{-1} respectively. The 430 cm^{-1} peak may be attributed to Ti–O–Ti vibration.[25] The ST10 and ST55 films were further heated to 700 °C in order to confirm the peak appearing at 935 cm^{-1} is due to the Si–O–Ti vibration, which is often confused due to overlap with Si–OH. It has been observed that in case of ST10, the Si–OH peak is almost disappeared after heat treatment at 700 °C due to further silanol (Si–OH) condensation; on the contrary the ST55 film retains the intense peak at 935 cm^{-1} due to Si–O–Ti (Fig. 1c). The presence of Si–O–Ti in FTIR therefore confirms that some mol fraction of the added TiO_2 enters into the SiO_2 network. It is therefore clear from FTIR studies that the modification of the refractive indices of the SiO_2–TiO_2 mixed matrices arises from a uniform composite structure having a Si–O–Si, Si–O–Ti and Ti–O–Ti interconnecting network. A systematic increase of refractive index with increase of TiO_2 content also suggests the formation of a uniform SiO_2–TiO_2 network in the mixed films as also pointed out by other workers.[20]

The evolution of Au nanoparticles in the coating matrices was monitored using UV–visible spectroscopy and results are presented in Fig. 2a–f. The ST10 film showed an absorption peak in the 312 nm (Fig. 2a) region due to the presence of $AuCl_4^-$ inside the coatings.[26] This peak is due to the charge transfer between the Au and chloro ligands.[26] The formation of Au nanoparticles started when the coating was dried at 60–90 °C and, as a result of this, the intensity of $AuCl_4^-$ peak gradually weakened and SPR peak, due to Au nanoparticles, intensified. In all other cases (Fig. 2b–e), the $AuCl_4^-$ peak was not clearly observed due to the absorption of TiO_2 above 400 nm. However, a shoulder peak appearing at about 320 nm in all as-prepared and dried Ti-containing films can be attributed to the absorption of $AuCl_4^-$ ions along with absorption of Ti–acac chelate. It may be noted here that in the case of ST10 (pure silica, $SiO_2 : TiO_2 = 1 : 0$), the Au SPR peak is observed at 543 nm during drying even at 60 °C, and intensity of this peak is increased at 90 °C. The position of SPR is almost retained (542 nm) after heat treatment at 500 °C (Fig. 2a). The refractive index (Table 2) of the 90° dried ST10 film has been decreased from 1.468 to 1.411 after heat treatment at 500 °C indicating the formation of porous SiO_2

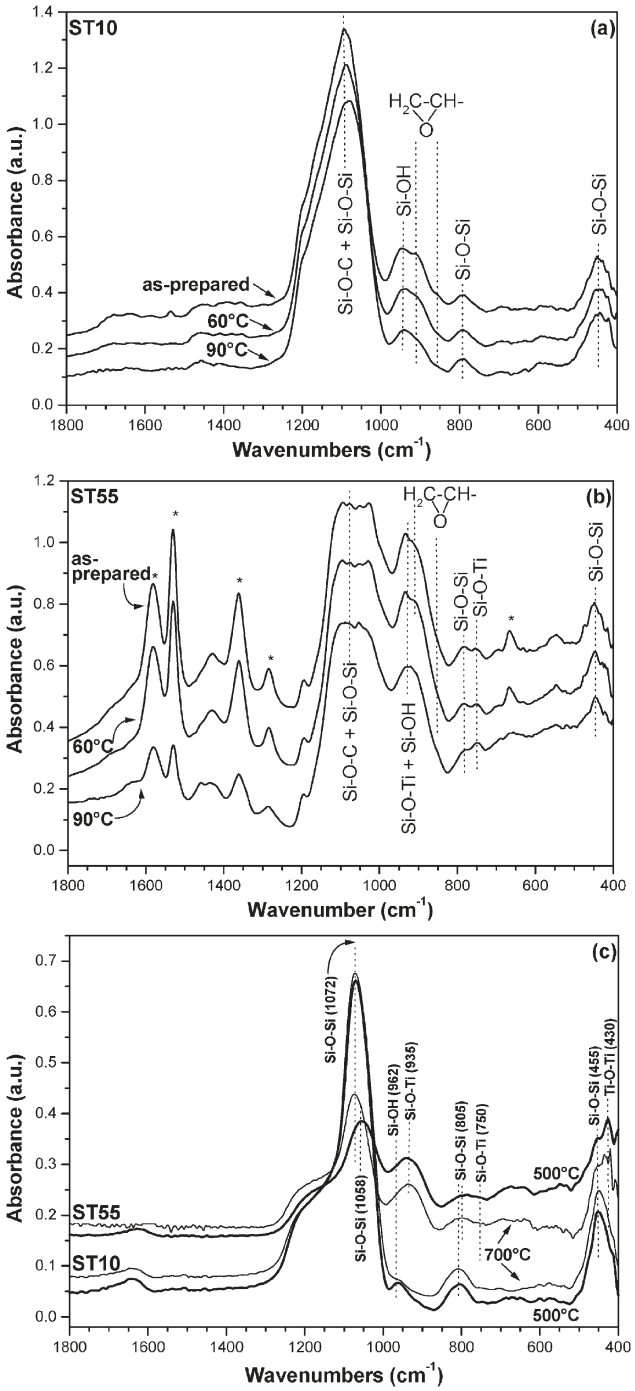

Fig. 1 FTIR spectra of Au doped films dried and heat treated at different temperatures: (a) ST10, (b) ST55 and (c) heat treated ST10 and ST55 films. Films were deposited on double side-polished (intrinsic, IR transparent) Si wafers.

film after the elimination of organics. However, the position of Au SPR remains more or less undisturbed. The formation of Au nanoparticles is also induced at 60 °C in the ST73 and ST55 films having compositions SiO_2 : TiO_2 = 7 : 3 and 1 : 1 respectively (Fig. 2b and c). Upon increasing the Ti concentration further (ST46 and ST39), we did not observe any Au SPR after drying at 60 °C, which indicates no noticeable Au nanoparticle generation at 60 °C. In these cases the Au SPR is observed at 90 °C (Fig. 2d and e). We have measured the refractive indices of undoped film samples (Table 2) after drying at 90 °C and observe an increase of the matrix refractive indices on going from ST10 (n = 1.468) to ST39 (n = 1.648). However, noticeable shifting of Au SPR due to such an increase of refractive index is not observed. The Au SPR only shifted from 543 nm (ST10) to 548 nm (ST39). On the contrary, when the Ti-containing films are heated at 500 °C for 30 min we observe, in all cases, a clear red-shifting of Au SPR due to an increase of matrix refractive indices (Fig. 2b–e). Accordingly the colour of the films changed after heat treatment at 500 °C. Fig. 2(f) shows the optical absorption spectra of all the film compositions (Table 1) heat treated at 500 °C. The shift of Au SPR from 542 nm to 600 nm is clearly seen on going from SiO_2 : TiO_2 = 1 : 0 (ST10) to 1 : 3 (ST39) due to the systematic increase in the refractive index of the matrices. As a consequence, different coloured coatings on the glass substrates were obtained: pink (ST10), magenta (ST73), violet (ST55), royal (ST46) and blue (ST39). A systematic red-shifting of the Au SPR position is therefore clearly established due to an increase in the refractive indices of the matrices. Therefore, the inorganic–organic hybrid approach not only prevented the films cracking due to increased thickness, but also helped to generate very uniform colours after heat treatment at 500 °C. Fig. 3 shows a photo of heat treated (500 °C) films on soda-lime–silica glass substrates. All films are crack-free except ST39 where fine cracks are observed due to high TiO_2 content (75 mol%) in the matrix. The photo clearly shows uniform coloration and a systematic colour change due to an increase in the refractive index of the coating matrices. The uniform coloration is an indication that the structure of composite SiO_2–TiO_2 matrices and distribution of the embedded Au nanoparticles are very uniform. The homogeneity of Au nanoparticles in the coating matrices was qualitatively verified by comparing the absorbance of the Au SPR peak at five different positions for films ST10, ST73, ST55 and ST46 of dimensions 2 cm × 1 cm (the edges were not used for measurement). The scatter in the Au SPR absorbance due to these different positions in all the samples was less than 2%, indicating a homogeneous distribution of the Au nanoparticles in the matrices.

It was reported[17] that the decomposition of $AuCl_4^-$ leading to the formation of Au nanoparticles occurs at around 200 °C in the case of alkoxide (tetraethyl orthosilicate, methyltriethoxysilane, titanium tetrabutoxide *etc.*) derived coatings. However, in our case, the formation of Au nanoparticles is induced at 60–90 °C. The reduction of $AuCl_4^-$ to Au metal nanoparticles is most probably facilitated during the epoxy polymerization through a ring opening mechanism[23,27] at 60–90 °C. It may also be noted here that although the refractive indices of films dried at 90 °C are increased, the plasmon absorption of Au nanoparticles has little effect on this. It is known that the plasmon absorption is mainly governed by the refractive index of matrix which is actually adjacent to the nanoparticles.[5,11] So it is likely that in all of our films dried at 60–90 °C, Au nanoparticles remain in a more or less identical environment surrounded by matrices having more or less identical refractive indices. Up to 90 °C, these films consist of an interconnecting inorganic (–Si–O–Si–,

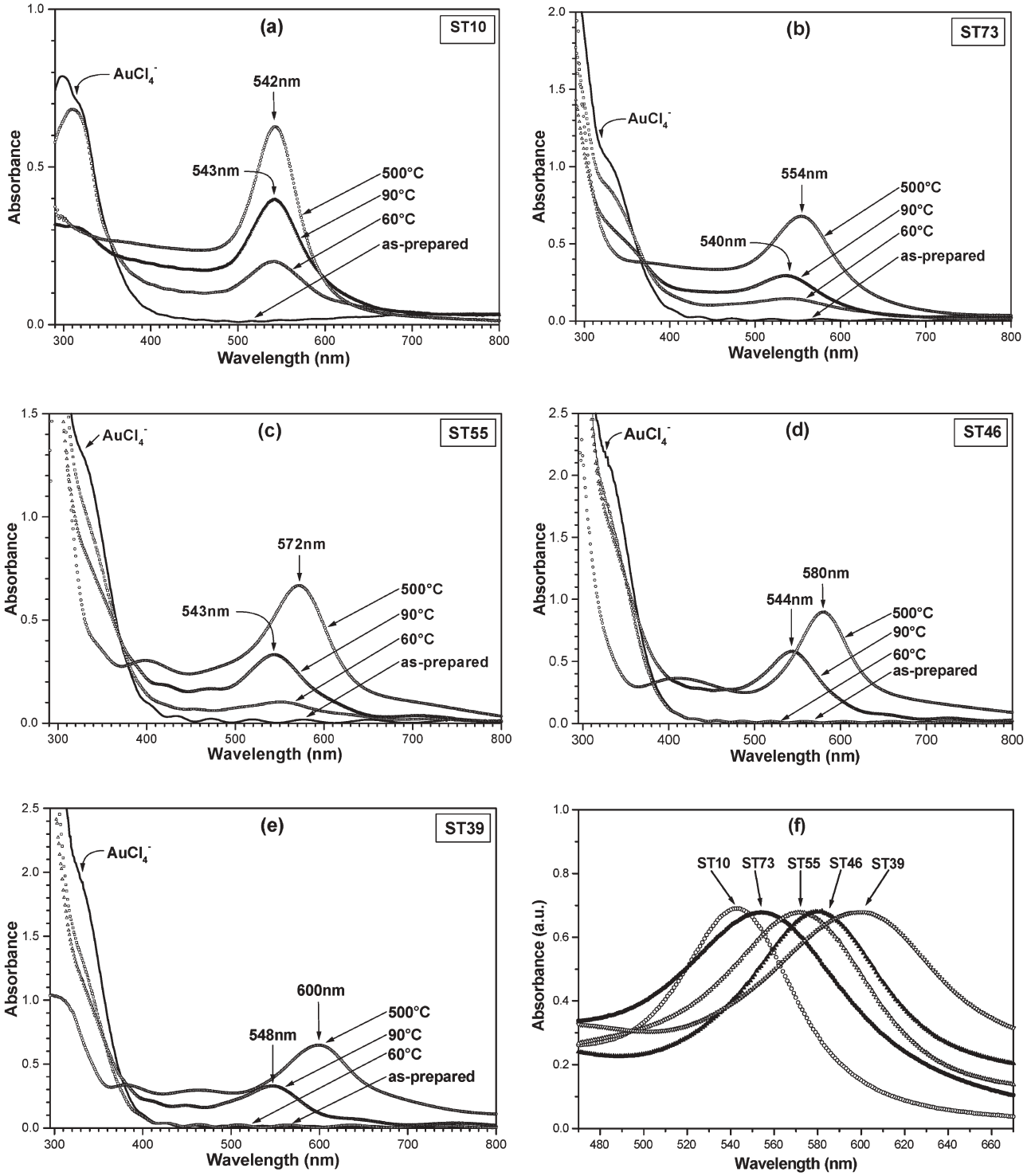

Fig. 2 Optical absorption spectral evolution during the formation of Au nanoparticles monitored by UV–Visible spectrometer: (a) ST10, (b) ST73, (c) ST55, (d) ST46, (e) ST39 films and (f) spectra of all films heat treated at 500 °C. The films were deposited on soda-lime–silica glass substrates and both sides of the substrate were coated. The film thickness of the final heat treated (500 °C) samples was 550 ± 10 nm (ST10), 600 ± 10 nm (ST73), 350 ± 5 nm (ST55), 290 ± 5 nm (ST46) and 250 ± 5 nm (ST39) respectively.

–Si–O–Ti–) and organic (poly(ethylene oxide)) network.[21] As the inorganic network has a higher refractive index, it is expected that the Au nanoparticles will remain in close proximity to the poly(ethelene oxide) network and, as a result, noticeable shifting of Au SPR is not observed. This also supports that Au nanoparticles form in close proximity to epoxy groups. After heat treatment at 500 °C all organics are burnt off and the Au nanoparticles are then embedded in a uniform SiO_2–TiO_2 network; the position of the Au SPR is then controlled by the matrix refractive indices. Is this

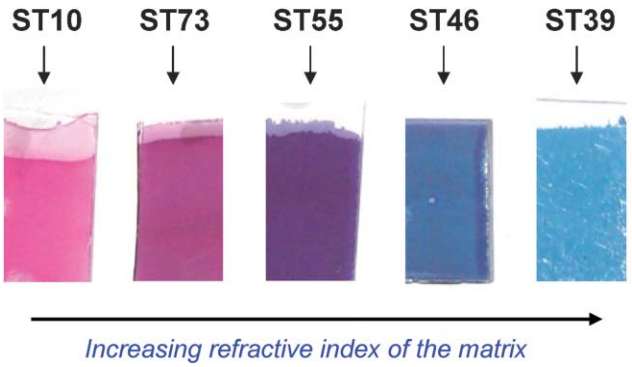

Fig. 3 Photo showing Au nanoparticle doped coloured films on soda-lime–silica glass substrates heat treated at 500 °C. The position of Au SPR was tailored by changing the refractive index of the matrix.

systematic shifting of the Au SPR only caused by the change in the refractive index of the matrix, or are other factors (size, shape *etc.*) mentioned in the introduction also playing significant roles? To answer this question we used X-ray diffraction (XRD) and transmission electron microscopy (TEM). The XRD does not show any peaks related to crystalline TiO_2 phases, but it does show broad FCC Au peaks for all the heat treated (500 °C) coatings (the XRD data are shown in the electronic supplementary information (ESI)† Figs. A and B). This result confirms that Au nanoparticles are embedded in amorphous glassy matrices. The results of the TEM analysis of samples ST10 and one representative Ti-containing film ST46 are summarized in Fig. 4. Figs. 4a and b show the TEM images taken from ST10 and ST46 films dried at 90 °C; in both the cases near-spherical Au nanoparticles of average diameters of about 18.5 nm are observed. This indicates that inclusion of a large amount of TiO_2 in SiO_2 has no significant influence on the development of the size and shape of the Au nanocrystals. Figs. 4c and d show the TEM images taken from the corresponding heat treated (500 °C) ST10 and ST46 films. A selected area diffraction pattern taken from larger clusters of the ST10 film shows (inset of Fig. 4c) spots attributed to FCC Au. The inset of Fig. 4d shows a high resolution image of one Au nanocrystal taken from ST46 film. The high resolution image clearly shows Au (111) lattice fringes. It is interesting to observe that heat treatment at 500 °C causes no significant enlargement in either sample, though the matrix refractive index increased from 1.411 (ST10) to 1.862 (ST46). An average particle size of about 19.5 and 21.5 nm was found in ST10 and ST46 films respectively. Therefore TEM confirms that the systematic shifting of the Au SPR observed in the present study is mainly due to the systematic increase of the refractive indices of embedding matrices.

We have tried to compare the observed Au SPR positions with respect to the refractive indices by theoretical simulation using the Mie theory.[5] An average cluster size of $r = 10$ nm was taken from the TEM study. The simulation was based on the following assumptions: (i) the clusters are non-interacting and perfectly spherical; (ii) the dielectric functions of metallic nanoclusters are corrected for finite size and (iii) the refractive index of the host is assumed to be constant over the whole range of wavelengths considered and the small absorption of the host (the imaginary part of the refractive index) has been neglected. Fig. 5 shows the result of the calculated Au SPR position with respect to the matrix refractive indices along with the observed position. The constant difference between the calculated and observed Au SPR position could be due to the anisotropy of the Au nanoparticles and some distribution of particle sizes as observed by TEM. It has been reported that if nanoparticles are not perfectly spherical, red-shifting/broadening of SPR could be observed.[6,28] Heat treated (500 °C) ST10 and ST46 films (marked by an arrow in Fig. 4c and in

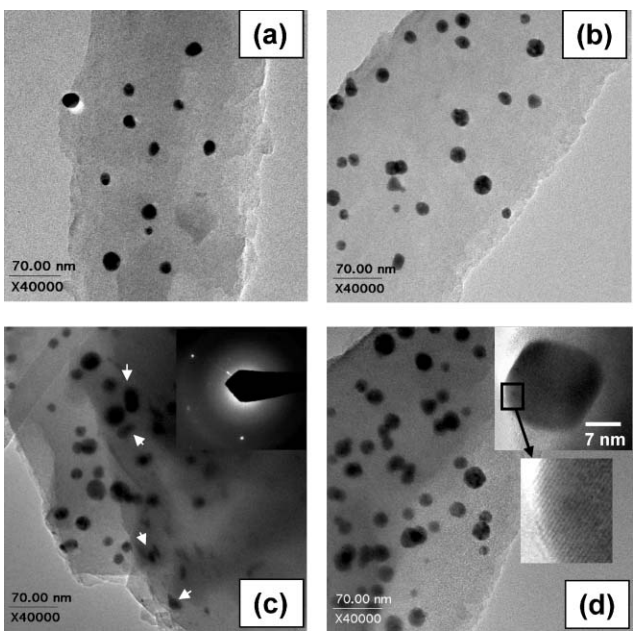

Fig. 4 TEM image showing Au nanoparticles embedded in films (a) ST10 dried at 90 °C, (b) ST46 dried at 90 °C, (c) ST10 heat treated at 500 °C and (d) ST46 heat treated at 500 °C. The inset of Figs. (c) and (d) shows a selected area diffraction pattern and a high resolution image respectively.

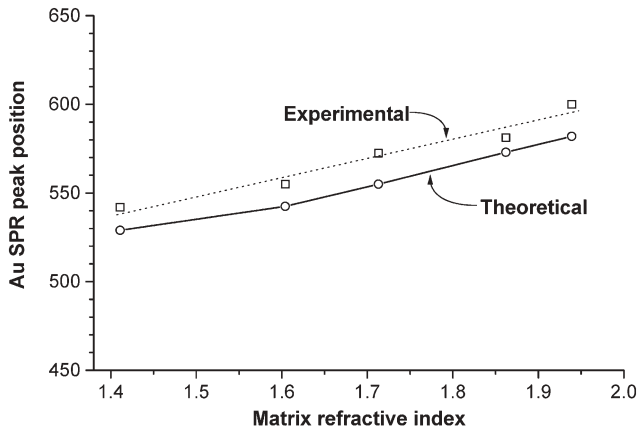

Fig. 5 Plots showing Au SPR positions with respect to the matrix refractive indices. Both the experimentally observed Au SPR positions and the corresponding theoretical simulation based on Mie theory are shown.

the high resolution image, inset Fig. 4d) show deviations of Au nanoparticles from spherical shapes.

Conclusions

Au nanoparticle doped SiO_2 and mixed SiO_2–TiO_2 glassy films of different colours were synthesised on ordinary glass substrates using an inorganic–organic hybrid sol-gel route followed by thermal annealing at 500 °C. Our results show that using this approach, the position of the Au SPR band in the visible wavelength region can be controlled easily and systematically by changing the matrix refractive indices and, as a result, fine tuning of the colour is possible. Formation of Au nanoparticles embedded in glassy film matrices having different Au SPR absorption positions in the visible wavelength of light, but similar particle size distributions is noteworthy and could be of potential technological interest for optical switching applications using lasers of different wavelengths.

Acknowledgements

Financial support from the Department of Science and Technology (DST), Govt. of India, in the form of a project (SR/S5/NM-13/2002) under *'Nanomaterials Science and Technology Initiative'* (NSTI) programme is thankfully acknowledged. Thanks are also due to Prof. C. J. Brinker, University of New Mexico for helping with TEM and ellipsometric characterisation and Dr G. Mattei, Padova University for theoretical simulation. The authors thank Dr H. S. Maiti, Director, CG&CRI for his kind permission to publish this work.

References

1 M. El-Sayed, *Acc. Chem. Res.*, 2001, **34**, 257.
2 R. Jin, Y.-W. Cao, C. A. Mirkin, K. L. Kelly, G. C. Schatz and J. G. Zheng, *Science*, 2001, **294**, 1901.
3 V. F. Puntes, D. Zanchet, C. K. Erdinmez and A. P. J. Alivisatos, *J. Am. Chem. Soc.*, 2002, **124**, 12874.
4 Y. Sun, B. Mayers and Y. Xia, *Nano Lett.*, 2003, **3**, 675.
5 U. Kreibig and M. Vollmer, *Optical Properties of Metal Clusters*, Springer, Berlin, 1995.
6 G. De and C. N. R. Rao, *J. Mater. Chem.*, 2005, **15**, 891.
7 G. De and C. N. R. Rao, *J. Phys. Chem. B*, 2003, **107**, 13597.
8 G. De, G. Mattei, P. Mazzoldi, C. Sada, G. Battaglin and A. Quaranta, *Chem. Mater.*, 2000, **12**, 2157.
9 G. De, *J. Sol-Gel Sci. Technol.*, 1998, **11**, 289.
10 F. Gonella, G. Mattei, P. Mazzoldi, G. Battaglin, A. Quaranta, G. De and M. Montecchi, *Chem. Mater.*, 1999, **11**, 814.
11 W. Cheng and E. Wang, *J. Phys. Chem. B*, 2004, **198**, 24.
12 G. Mie, *Ann. Phys.*, 1908, **25**, 377.
13 R. H. Doremus, *Langmuir*, 2002, **18**, 2436.
14 H. Hache, D. Ricard and C. Flytzanis, *J. Opt. Soc. Am.*, 1986, **B3**, 1647; C. Flytzanis, F. Hache, M. C. Klein, D. Ricard and Ph. Roussignol, *Prog. Opt.*, 1991, **29**, 321; T. Tokizaki, A. Nakamura, S. Kaneko, K. Uchida, S. Omi, H. Tanji and Y. Asahara, *Appl. Phys. Lett.*, 1994, **65**, 941.
15 G. De, L. Tapfer, M. Catalano, G. Battaglin, F. Caccavale, F. Gonella, P. Mazzoldi and R. F. Haglund, Jr., *Appl. Phys. Lett.*, 1996, **68**, 3820; P. P. Kiran, B. N. S. Bhaktha, D. N. Rao and G. De, *J. Appl. Phys.*, 2004, **96**, 6717.
16 Y-P. Sun, J. E. Riggs, K. B. Henbest and R. B. Martin, *J. Nonlin. Opt. Phys. Mater.*, 2000, **9**, 481.
17 P. Innocenzi, H. Kozuka and S. Sakka, *J. Sol-Gel Sci. Technol.*, 1994, **1**, 305.
18 F. Del Monte, P. Cheben, C. P. Grover and J. D. Mackenzie, *J. Sol-Gel Sci. Technol.*, 1999, **15**, 73; W. Que, Y. Zhou, Y. L. Lam, Y. C. Chan, S. D. Cheng, Z. Sun and C. H. Kam, *J. Sol-Gel Sci. Technol.*, 2000, **18**, 73.
19 G. De and S. K. Medda, *Indian Pat. Appl.* 346NF2003.
20 H. Schroeder, *Phys. Thin Films*, 1969, **5**, 87–141; C. J. Brinker and M. S. Harrington, *Sol. Energy Mater.*, 1981, **5**, 159.
21 G. De and D. Kundu, *Chem. Mater.*, 2001, **13**, 4239.
22 S. K. Medda, D. Kundu and G. De, *J. Non-Cryst. Solids*, 2003, **318**, 149.
23 P. Innocenzi, G. Brusatin, M. Guglielmi and R. Bertani, *Chem. Mater.*, 1999, **13**, 4239; K. Dean, W. D. Cook, P. Bruchill and M. Zipper, *Polymer*, 2001, **42**, 3589.
24 G. De, A. Chatterjee and D. Ganguli, *J. Mater. Sci. Lett.*, 1990, **9**, 845; A. Léaustic, F. Babonneau and J. Livage, *Chem. Mater.*, 1989, **1**, 240.
25 Q. Fang, M. Meier, J. J. Yu, Z. M. Wang, J.-Y. Zhang, J. X. Wu, A. Kenyon, P. Hoffmann and I. W. Boyd, *Mater. Sci. Eng., B*, 2003, **105**, 209.
26 K. Torigoe and K. Esumi, *J. Phys. Chem. B*, 1999, **203**, 2862.
27 S. Warwel, B. Wiege, E. Fehling and M. Kunz, *Eur. Polym. J.*, 2000, **36**, 2291.
28 A. I. Kirkland, D. A. Jefferson, D. G. Duff, P. P. Edwards, I. Gameson, B. F. G. Johnson and D. J. Smith, *Proc. R. Soc. London, Ser. A*, 1993, **440**, 589.

